Ain Shams Engineering Journal (2014) 5, 137–148

Ain Shams University

Ain Shams Engineering Journal

www.elsevier.com/locate/asej
www.sciencedirect.com

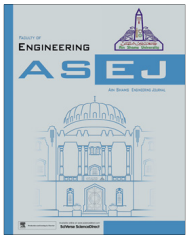

ELECTRICAL ENGINEERING

Modeling and investigation of Gulf El-Zayt wind farm for stability studying during extreme gust wind occurrence

Omar Noureldeen [a,*], **Ahmed Rashad** [b]

[a] *Electrical Engineering Department, Faculty of Engineering, South Valley University, Qena, Egypt*
[b] *Upper Egypt Electricity Distribution Company, Qena Rural Electrification Sector, Egypt*

Received 26 March 2013; revised 29 August 2013; accepted 19 September 2013
Available online 20 October 2013

KEYWORDS

Extreme gust wind;
DFIG;
Wind farm;
Active power;
Reactive power

Abstract This paper investigates the impact of extreme gust wind as a case of wind speed variation on a wind farm interconnected electrical grid. The impact of extreme gust wind speed variation on active and reactive power of the wind farms is studied for variable speed wind farm equipped with Doubly Fed Induction Generators (DFIGs). A simulation model of the under implementation 120 MW wind farm at Gulf El-Zayt region, Red Sea, Egypt, is simulated as a case study. A detailed model of extreme gust wind speed variation is implemented and simulated, using MATLAB/Simulink toolbox, based on International Electrotechnical Commission IEC 61400-1 and climate characteristic of Gulf El-Zayt site. The simulation results show the influence of different extreme gust wind speed variations on the fluctuation of active power and reactive power at the Point of Common Coupling (PCC) of the studied wind farm.

1. Introduction

Wind power generation systems are already popular in the world, and the utilization of this renewable energy source is expanding rapidly. Because of its attractive advantages, including zero-CO_2 emissions and low operation cost, the penetration of wind power generation systems is increasing in spite of the variable characteristics of wind speed. The DFIG concept has become one of the most favorable options in modern wind power market. The DFIG wind turbine consists of wound rotor induction generator, that is connected to the turbine blades via a gearbox. The stator of a wound rotor generator is connected directly to the grid, whereas the rotor is connected to the grid through two back-to-back converters with a common DC link capacitor bank. This arrangement allows for power in the rotor to be at a different frequency than that of the grid frequency, thereby allowing for speed control by adjusting this frequency. There are several advantages of the DFIG system, where the variable speed allows for optimal power to be extracted for a wide range of wind speeds. Both active and reactive power can be controlled independently. Also, reactive power can be supplied by the generator to support grid voltages. The disadvantages of the DFIG are the harmonics generated by the power converter need to be filtered to comply with grid connection specifications [1]. The wind itself

* Corresponding author. Tel.: +20 966711300, mobile: +20 1273139996.
E-mail address: omar_noureldeen@svu.edu.eg (O. Noureldeen).

Peer review under responsibility of Ain Shams University.

ELSEVIER Production and hosting by Elsevier

2090-4479 © 2013 Production and hosting by Elsevier B.V. on behalf of Ain Shams University.
http://dx.doi.org/10.1016/j.asej.2013.09.011

is a variable source of energy. The ability of a wind turbine to extract power from varying wind is a function of three main factors – the wind power availability, the power curve of the generator, and the ability of the turbine to respond to wind fluctuations. Wind turbines are typically be placed in rows perpendicular to the prevailing wind direction. The distance between the wind turbines in each row and the distance between the rows depend on the rotor diameter. In a uniform wind direction the distance between turbines in rows and columns is approximately equal to 5 times of rotor diameter. In case of predominate wind direction, the recommended turbine spacing is equal to 8–12 times of rotor diameter in rows apart in the windward direction, and equal to 1.5–3 times of rotor diameter a part in the crosswind direction [2]. The wind turbines with tall hub heights can extract large amounts of energy from the atmosphere because they are likely to encounter higher wind speeds, but they face challenges given the complex nature of wind flow and turbulence at these heights in the boundary layer. Depending on whether the boundary layer is stable, neutral, or convective, the mean wind speed, direction, and turbulence properties may vary greatly across the tall turbine swept area (40–120 m above ground level) [3]. This variability can cause tall turbines to produce difference amounts of power during time periods with identical hub height wind speeds. The strategy of New and Renewable Energy Authority of Egypt NREA, which was approved in February 2008, aims to the contribution of renewable energies by 20% of the total electricity generation by the year 2020, including 12% contribution from wind energy, translating about 7200 MW grid-connected wind farms. Gulf El-Zayt site at the Red Sea region, it is classified as an excellent wind speed site which it reaches 10.5 m/s as average wind speed over one-year period at 25 m above ground level and it can host about 3000 MW wind power plants. However, technical considerations suggest that the area cannot absorb more than 2000 MW. The target is to develop the overall area until 2024. One of those projects under implementation is a 120 MW wind farm as a first step (possibly upgraded to 400 MW), and it sited at Gulf El-Zayt site [4]. This project is expected to be completed and operated in the end of 2014. This wind farm will produce approximately 500.000 MW h contributing to partially cover 35% of the Suez cement factory energy needs. In this paper, the effect of extreme gust wind speed variation on the stability of Gulf El-Zayt wind farm is investigated for different operation conditions by monitoring the variations in wind farm active and reactive power. To investigate the impacts of extreme gust wind speed variations on the stability of the studied wind farm, a simulation model of a 120 MW wind farm connected to a grid is investigated. Also, a detailed model of extreme gust wind is investigated and simulated according the recorded average wind speed over one-year period at Gulf El-Zayt site and the standard IEC 61400-1. The impacts of extreme gust wind speed variation on the stability of the simulated wind farm are studied by monitoring the active power and reactive power at the Point of Common Coupling (PCC) bus of the studied system. The complete wind farm connected-grid model, includes the extreme gust wind model, the aerodynamic model of the wind turbine, the model of electrical component namely the DFIG, transmission line model, transformers. All the model components of the wind farm connected-grid are built with standard electrical component models using the MATLAB SimPowerSystems toolbox and 32 bit windows 7 platform.

2. Simulation of extreme gust wind

In this paper, the extreme gust wind speed variations are simulated by simulating the extreme wind conditions as specified in IEC 61400-1 [5,6]. The extreme wind conditions include peak wind speeds due to gust and rapid changes in wind speed. The mathematical model of the extreme gust wind depends on the climatic characteristics in the site where the wind farm is located. The wind profile is the average wind speed as a function of height, z, above the ground. The normal wind speed profile is given by

$$V(z) = V_{hub}\left(\frac{z}{z_{hub}}\right)^{\alpha} \tag{1}$$

where (z) is the average wind speed at height z above the ground (m/s), z_{hub} is the hub height of the wind turbine (m), and V_{hub} is the wind speed at hub height averaged over ten minutes (m/s). The power law exponent, α is assumed to be 0.25 which is the standard value for the Egyptian terrain and wind conditions [7,8]. The wind speed is defined for a recurrence period of N years by the following equation [6]:

$$V(z,t) = \begin{bmatrix} V(z) - 0.37V_{gustN}\left(\sin\left(\frac{3\pi t}{T}\right)\right)\left(1-\cos\left(\frac{2\pi t}{T}\right)\right) & for \rightarrow T_{start} \leqslant t \leqslant T_{final} \\ V(z) & for \rightarrow t < T_{start} \ and \ t > T_{final} \end{bmatrix} \tag{2}$$

where T_{start} is the time of the beginning of the gust, T_{final} is the time of the demise of the gust, and T is the gust characteristics time (s), it equals to 10.5 s for a recurrence period N equal to 1 year and it equals to 14 s for a recurrence period N equal to 50 years. V_{gustN} is the largest extreme gust magnitude with an expected recurrence period of N year and it can be given by

$$V_{gustN} = \beta\left(\frac{\sigma}{1+0.1\left(\frac{D}{A}\right)}\right) \tag{3}$$

where β is the parameter for extreme direction change model, it equal to 4.8 for a recurrence period N equal to 1 year, and it equal to 6.4 for a recurrence period N equal to 50 years, D is the rotor diameter (m), and A is the turbulence scale parameter (m) where it can be given by

$$A = \begin{bmatrix} 0.7z_{hub} & \text{for} & z_{hub} < 30 \text{ m} \\ 21 \text{ m} & \text{for} & z_{hub} \geqslant 30 \text{ m} \end{bmatrix} \tag{4}$$

finally σ is the standard deviation of longitudinal wind velocity and it can be given by

$$\sigma = \frac{I_{15}(15 + aV_{hub})}{(a+1)} \tag{5}$$

where I_{15} is the characteristic value of the turbulence intensity at a 10 min average wind speed of 15 m/s, and a is the slop parameter of turbulence intensity.

The wind turbine generator system classes are used to determine the suitable turbine for the normal wind conditions of a particular site [5]. The wind classes are mainly defined by the average annual wind speed which is measured at the turbine hub height, the speed of extreme gusts that could occur over N years, and how much turbulence there is at the wind site. The wind turbine generator system classes are defined by IEC 61400-1 correspond to high, medium and low wind speed as shown in Table 1. It shows that, there are four classes for wind turbine generators. In the case of a wind turbine that is designed for lower wind speeds, the design loads are going to

Table 1 Wind turbine generator system classes.

Class	V_{ave} (m/s)	A (high turbulence)		B (low turbulence)	
		I_{15}	a	I_{15}	a
I	10	0.18	2	0.16	3
II	8.5	0.18	2	0.16	3
III	7.5	0.18	2	0.16	3
IV	6	0.18	2	0.16	3

Table 2 Wind turbine generator specifications.

Rated power (MW)	2
Cut-in wind speed (m/s)	3
Rated wind speed (m/s)	13
Cut-out wind speed (m/s)	25
Rotor diameter (m)	76.42
Rotor area (m^2)	4587
Blade length (m)	37
Hub height (m)	70

be smaller, therefore its blades are larger and hub height is taller. As a result, bigger rotors of class IV capture more wind energy and yield higher capacity factors compared to other classes. In this paper, these classes are used to choose a suitable wind turbine generator for climate characteristics of Gulf El-Zayt site. Wind Atlas of Egypt concludes that the yearly average wind speed at Gulf El-Zayt site is about 10.5 m/s measured at a height above the ground of 25 m. The NREA annual report, 2011, reported that the suggested capacity of each wind turbine generator is 2 MW [9]. Also, a feasibility study for a large wind farm at Gulf El-Zeit site, 2008, reported that the maximum blade tip heights of about 100 m and it is proposed to limit the maximum tip height to 110 m to be in accordance with the ornithological study and still allow wind turbines up to 2.5 MW. In order to achieve this study, 2 MW wind turbine generator with a hub height of 70 m and rated wind speed of 13 m/s is used as a suitable generator for Gulf El-zayt site. Where the calculated hub wind speed based recorded average wind speed of Gulf El-Zayt site using Eq. (1) is about 13.5 m/s at a height of 70 m above the ground level. The specifications of the suggested 2 MW wind turbine generator are illustrated in Table 2 [10]. The specifications of the 2 MW wind turbine generator, the wind turbine generator parameters of class 1 and the average wind speed at wind farm site are used to simulate the extreme gust wind speed variations at the hub height according to IEC 61400-1. Eq. (2) is simulated using MATLAB-Simulink toolbox to generate extreme gust wind speed variations which will be used to investigate the stability of studied wind farm. Fig. 1 shows the flowchart of the achieved Simulink program to generate data of different extreme gust wind speeds.

3. Models of wind turbine system

3.1. Wind turbine model

The mechanical power and the aerodynamic torque developed by a wind turbine are given by [11,12]

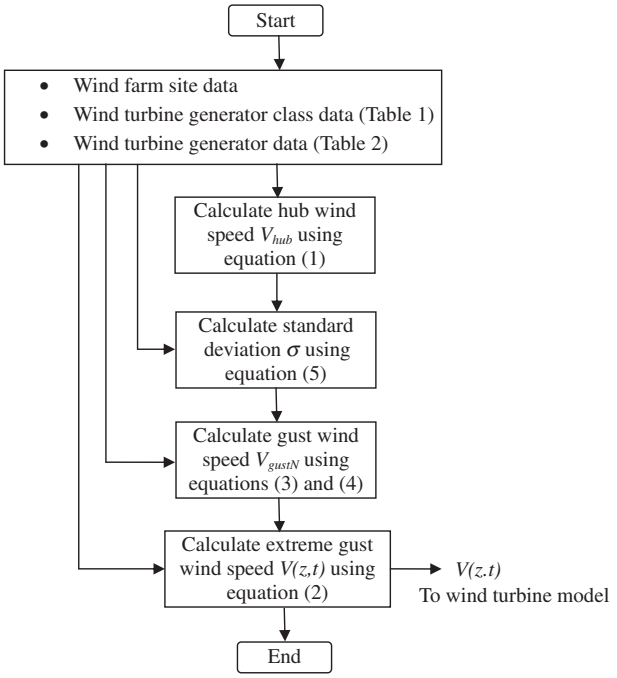

Figure 1 Flowchart of extreme gust wind calculation.

$$P_w = \frac{\pi \rho r^2}{2} V_{(z,t)}^3 C_p(\lambda, \theta) \tag{6}$$

where P_w is the mechanical output power captured from the turbine (W), ρ is the air density (nominally it equals 1.225 kg/m^3), r is the radius of the turbine (m), $V_{(z,t)}$ is the wind

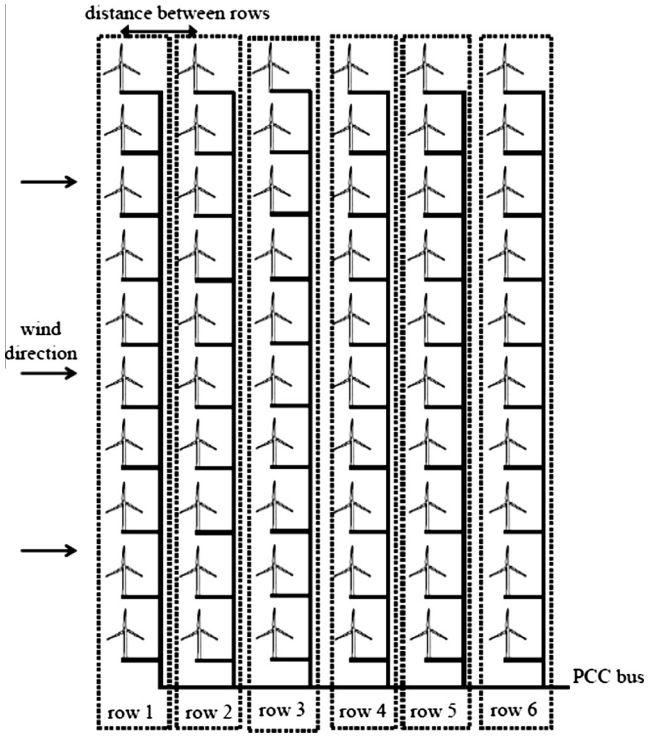

Figure 2 Layout of the simulated wind farm.

speed (m/s), C_P is the power coefficient of the wind turbine, θ is the pitch angle and λ is the tip speed ratio [13–15]. Where the tip speed ratio is defined as

$$\lambda = \frac{\omega_m r}{V_{(z,t)}} \tag{7}$$

where ω_m is the angular speed of turbines (rad/s). One of the methods used to calculate the power coefficient C_P by using a generic equation is [16–18]:

$$C_p(\lambda,\theta) = 0.5176\left(\frac{116}{\lambda_i} - 0.4\theta - 5\right)e^{\frac{-0.0068}{\lambda_i}} + 0.0068\lambda \tag{8}$$

where λ_i is given by:

$$\frac{1}{\lambda_i} = \frac{1}{\lambda + 0.08\theta} - \frac{0.035}{\theta^3 + 1} \tag{9}$$

The power coefficient C_P represents the fraction of the power in the wind captured by the turbine and its maximum value theoretically is equal to 0.59. In practical design the maximum value of C_P is between 0.4 and 0.5 for high speed two blade wind turbine and between 0.2 and 0.4 for low speed turbines with more blades [2].

3.2. Generator model

The stator and rotor voltage equations of a wounded rotor induction generator in the arbitrary two axes reference frame (d–q frames) are as follows, where the quantities on the rotor side are referred to the stator side. The used subscripts are defined as follows: d: d axis quantity, q: q axis quantity, r: rotor quantity, s: stator quantity [19].

$$v_{ds} = r_s i_{ds} + \frac{d\psi_{ds}}{dt} - \omega\psi_{qs} \tag{10}$$

$$v_{qs} = r_s i_{qs} + \frac{d\psi_{qs}}{dt} + \omega\psi_{ds} \tag{11}$$

$$v_{dr} = r_r i_{dr} + \frac{d\psi_{dr}}{dt} - (\omega - \omega_r)\psi_{qr} \tag{12}$$

$$v_{qr} = r_r i_{qr} + \frac{d\psi_{qr}}{dt} + (\omega - \omega_r)\psi_{dr} \tag{13}$$

$$\psi_{ds} = L_s i_{ds} + L_m i_{dr} \tag{14}$$

$$\psi_{qs} = L_s i_{qs} + L_m i_{qr} \tag{15}$$

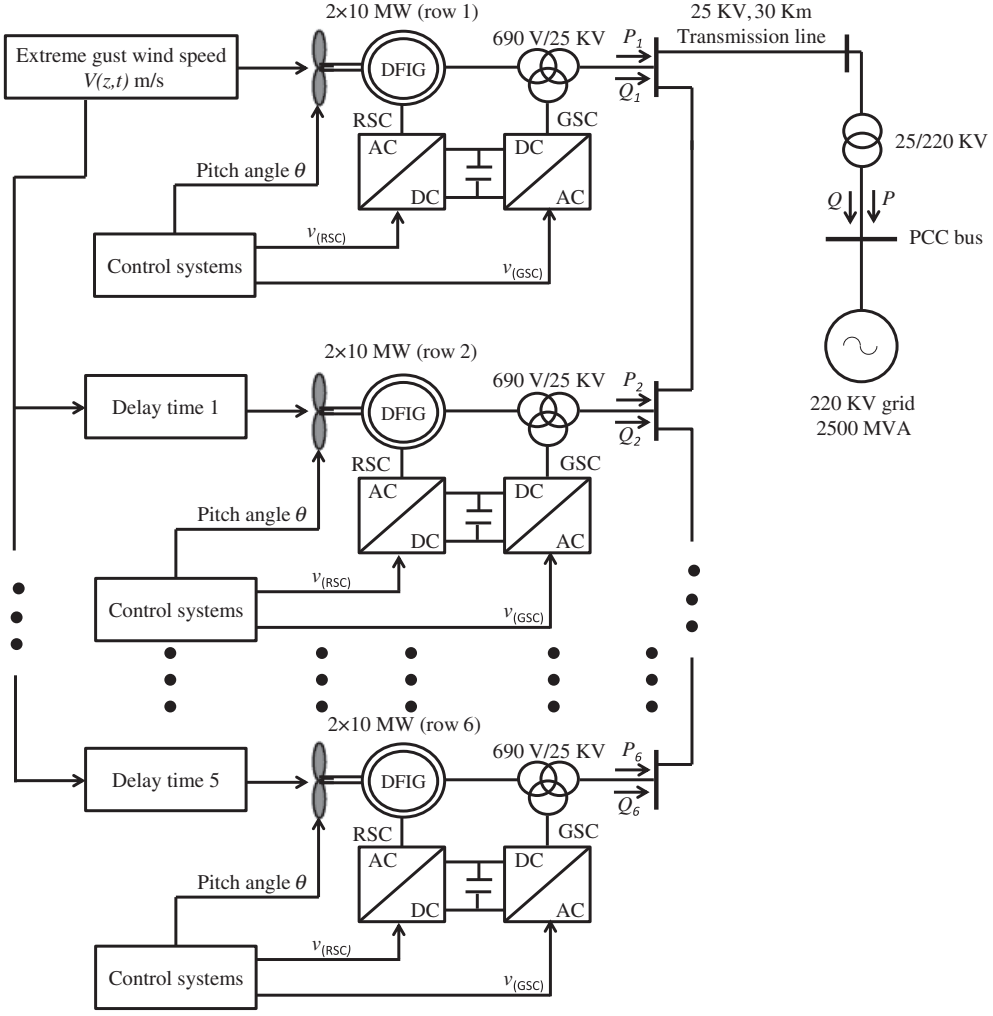

Figure 3 Single line diagram of the simulated wind farm.

$$\psi_{dr} = L_r i_{dr} + L_m i_{ds} \tag{16}$$

$$\psi_{qr} = L_r i_{qr} + L_m i_{qs} \tag{17}$$

$$L_s = L_{ls} + L_m \tag{18}$$

$$L_r = L_{lr} + L_m \tag{19}$$

where $_{ds}$, $_{qs}$, $_{dr}$, $_{qr}$, i_{ds}, i_{qs}, i_{dr}, i_{qr} and ψ_{ds}, ψ_{qs}, ψ_{dr}, ψ_{qr} are voltages (V), current (A) and flux linkages (Wb) of the stator and rotor in d–q axis, r_s and r_r are the resistances of the stator and rotor windings (Ω), L_s, L_r, L_m are the stator, rotor and mutual inductances (H), L_{ls}, L_{lr} are the stator and rotor leakage inductances (H), ω is the speed of the reference frame (rad/s), ω_r is the electrical angular velocity of the generator rotor (rad/s). By calculating the apparent power and taking the real parts the following equations represent the stator-side and rotor-side active power respectively.

$$P_s = \frac{3}{2}(v_{ds} i_{ds} + v_{qs} i_{qs}) \tag{20}$$

$$P_r = \frac{3}{2}(v_{dr} i_{dr} + v_{qr} i_{qr}) \tag{21}$$

The rotor-side active power can also be found from the following equation

$$P_r = -sP_s \tag{22}$$

Accordingly the imaginary parts of the apparent power represent the stator-side and rotor-side reactive power respectively.

$$Q_s = \frac{3}{2}(v_{qs} i_{ds} - v_{ds} i_{qs}) \tag{23}$$

$$Q_r = \frac{3}{2}(v_{qr} i_{dr} - v_{dr} i_{qr}) \tag{24}$$

The mutual flux between rotor and stator produces magnetic energy, which is stored in the magnetic field. This energy produces an electromagnetic torque which is calculated as

$$T_e = \frac{3}{2} p L_m (i_{qs} i_{dr} - i_{ds} i_{qr}) \tag{25}$$

where p is the number of pole pairs.

4. Simulation and control of studied wind turbine generators

The studied wind farm has a total rated capacity of 120 MW and consists of 60 wind turbines equipped with DFIG, and each turbine has a capacity of 2 MW. The wind turbines are positioned in regular array of 10 by 6 where, 10 wind turbines are located in a row as shown in Fig. 2. In this paper, the distance between the rows along the main wind directions is varied between 3 and 8 times of rotor diameter for different studied cases. Wind speed direction is assumed to be perpendicular on wind turbine, meaning that the wind stream passes each 10 wind turbines at the same instant. Fig. 3 shows a single line diagram of the simulation model of 120 MW DFIG wind farm connected to a 25 kV distribution system exports power to a 220 kV grid with a capacity of 2500 MVA. In Egypt, the power plants and wind farms are connected to the Egyptian unified grid through the 220 kV power network [20]. To study the behavior of the wind turbine generators during passing of gust wind at different sites of wind farm, the wind farm is simulated by separated 6 generators each generates 20 MW, (2 MW multiplied by 10), as shown in Fig. 3. Among the other electrical parts of the wind farm, the transformers are of important in modeling because of relatively high impedances. Wind farm cable impedances, on the other hand, can be neglected [21]. The main data of DFIG generator and system parameters are described in Table 3. The DFIG consists of a wound rotor induction generator and an AC/DC/AC IGBT-based PWM converter. The stator winding is connected directly to the grid while the rotor is fed at variable frequency through the AC/DC/AC converter which consists of a rotor-side converter (RSC) and a grid-side converter (GSC). The direction of the power flow through the converters depends on the operating point of the generator. In the sub-synchronous operation mode, the stator of DFIG supplies power to the grid and also the slip power to the rotor via the slip rings and the power converters. In the super-synchronous operation mode, both the stator output power and the rotor slip power are fed into grid.

The control of DFIG is achieved by controlling the RSC, GSC and pitch angle as shown in Fig. 4. The details of the DFIG wind turbine control systems are given in [22,23]. The RSC is used to control the output power of the wind turbine and the voltage or reactive power at the grid terminals. The generated power is controlled to follow the predefined power-speed characteristics (tracking characteristic curve) [24]. Fig. 4(a) shows the schematic diagram of the RSC controller based on Proportional Integral (PI) controller. The variation in the maximum power with rotation speed ω_r of DFIG is predefined for each wind turbine. The actual wind turbine rotor speed ω_r is measured and the corresponding mechanical power P_r of the tracking characteristic curve is used as the reference power for the power control loop. The measured electri-

Table 3 DFIG data and system parameters.

DFIG parameters	
Rated power (MW)	2
Rated voltage (V)	690
Rated frequency (Hz)	60
Stator resistance (pu)	0.00707
Rotor resistance (pu)	0.005
Stator leakage inductance (pu)	0.171
Rotor leakage inductance (pu)	0.156
Mutual inductance (pu)	2.9
Lumped Inertia Constant (s)	5.04
25 kV Transmission line parameters	
Positive sequence resistance (ohm/km)	0.1153
Zero sequence resistance (ohm/km)	0.413
Positive sequence inductance (henries/km)	0.00105
Zero sequence inductance (henries/km)	0.00332
Positive sequence capacitance (farads/km)	11.33e−9
Zero sequence capacitance (farads/km)	5.01e−9
Wind turbine transformer	
Voltage ratio (kV)	0.69/25
Resistance (pu)	0.008
Reactance (pu)	0.0452
PCC transformer	
Voltage ratio (kV)	25/220
Resistance (pu)	0.005
Reactance (pu)	0.065

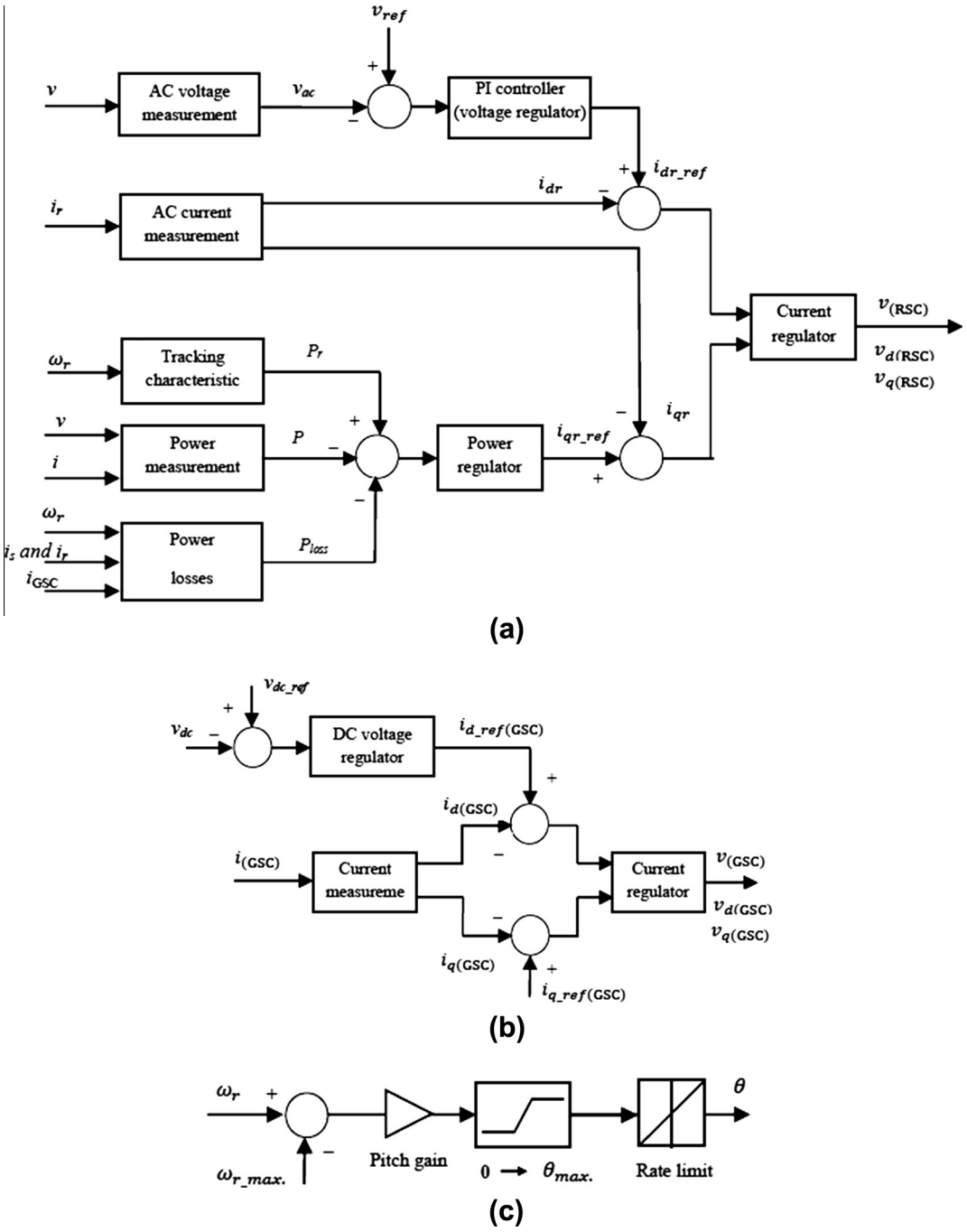

Figure 4 Schematic diagram of DFIG control systems (a) RSC controller. (b) GSC controller. (c) Pitch angle controller.

Table 4 Control system parameters.

Parameter	Gains	
	K_p	K_i
AC voltage regulator	1.25	300
Power regulator	1	100
Current regulator of RSC	0.3	8
DC voltage regulator	0.002	0.05
Current regulator of GSC	1	100
Pitch angle controller	500	–

cal output power P at the terminal of the wind turbine is added to the total of mechanical and electrical power losses P_{loss}, then the summation is compared with the reference power which obtained from the tracking characteristic. The operation of RSC controller requires i_{dr} and i_{qr} to follow the varying reference points i_{dr_erf} and i_{qr_erf}, that are determined by maintaining the output active power and stator-winding voltage at the setting values respectively. The required voltage for the RSC, $_{(RSC)}$, is derived by controlling the pu d and q axis currents of the RSC. The GSC controller is used to regulate the DC link voltage between both converters, and it is allowed to generate or absorb reactive power for voltage support requirements. As

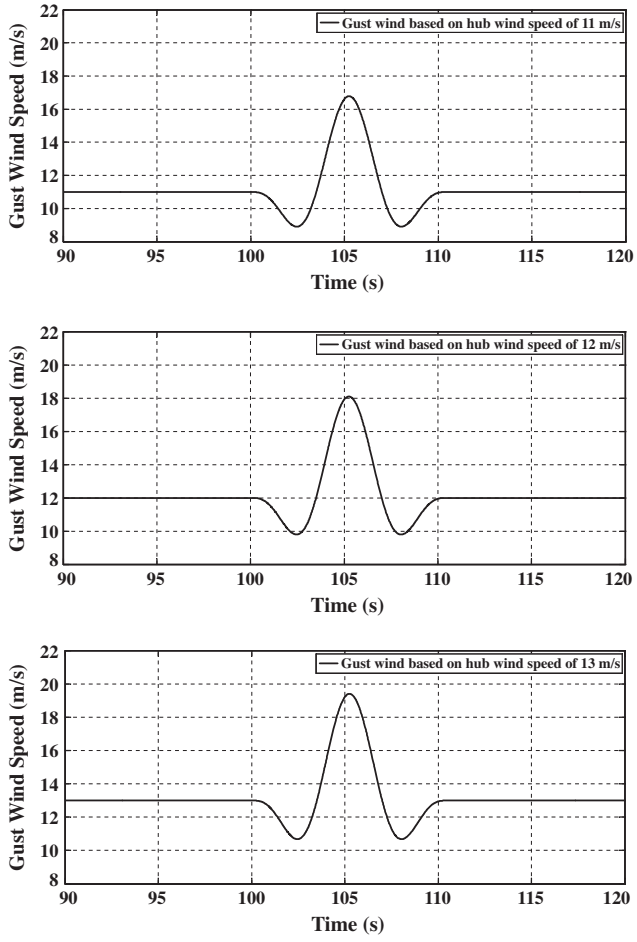

Figure 5 Wind speed variations for different gusts.

shown in Fig. 4(b), the pu d and q axis of the GSC, $i_{d(\mathrm{GSC})}$ and $i_{q(\mathrm{GSC})}$, have to track the reference points $i_{d\_ref\_(\mathrm{GSC})}$ and $i_{q\_ref\ (\mathrm{GSC})}$, that are determined by maintaining the DC link voltage at the setting value and keeping the output of GSC at unity power factor respectively. The required pu voltage of the GSC, $_{(\mathrm{GSC})}$, is derived by controlling the pu d and q axis currents of the RSC. Also, the wind turbine is equipped with a blade pitch control to limit the extracted power during conditions of high wind speeds. Fig. 4(c) shows the schematic diagram of pitch angler controller. The blade pitch angle control regulates the pitch angle of the wind turbine blades to determine the mechanical power that the turbine extracts from the wind. The blade pitch angle control is activated only when the wind speed is higher than the rated value. The wind turbine generators are operated in voltage regulation mode and the different control system parameters are illustrated in Table 4.

5. Simulation scenario and results

The wind farm stability will be studied for different extreme gust wind conditions. The extreme gust wind speed variation is simulated at different operation conditions assuming that the extreme gust wind occurs when the wind farm generators operate at a wind speed less than rated wind speed value, and when they operate at rated wind speed. The extreme gust wind speed variations are simulated as discussed in Section 2, based on different pre-gust wind speeds of 11, 12, and 13 m/s. The different simulated extreme gust wind speed variations are shown in Fig. 5. In a large wind farm, the time aspect of wind transport is an important consideration. Therefore, the stability of the simulated wind farm is studied when the extreme gust wind covers the wind farm generators gradually with a delay time depend on the peak value of extreme gust wind speed and the distance between the wind turbine rows. In this paper, the simulated extreme gust wind, (z,t), will cover each turbine generators row with a delay time, where it can be estimated as follows:

$$\text{Delay time (s)} = \frac{\text{Distance between rows (m)}}{\text{Peak gust wind speed (m/s)}} \tag{26}$$

The simulation is performed at different distances equal to 3, 5 and 8 times of rotor diameter between rows. The different studied cases are illustrated in Table 5. The wind farm wake effect is excluded in this study where it is affected by wind direction and wind farm layout. The wind direction depends on nature and can therefore not be modified; however, the wind farm layout can be modified to reduce the impact of the wake effect and thereby optimize wind farm performance [25]. As shown in Fig. 3, the PCC bus is the main bus of the wind farm which connects the wind farm with the grid, so in this paper this bus is taken as the monitoring point of the whole studied wind farm. The monitoring equipments (measurement equipments) are placed at the main bus PCC for monitoring the total generated active power from the wind farm to the grid and the total absorbed reactive power from the grid. Figs. 6–8 show the variations in active power and reactive power for different gusts when the distance between wind turbine rows equals to 3 times of rotor diameter. It is clear that, the pre-gust generated active power and the absorbed reactive power depend on the value of steady state wind speed. The generated active power equals to 83.7, 108.8, 117.1 MW and absorbed reactive power equals to 6.828, 6.327, 5.797 MVAR for pre-gust wind speeds of 11, 12, 13 m/s respectively.

During gust wind speed variation based on pre-gust wind speed of 11 m/s, the wind speed is fluctuated between 8.9 and 16.78 m/s for 10.5 s before it returns to steady state value. When the gust wind covers wind turbine generators of row 1, the active power at PCC bus is decreased to 82.07 MW, and then it increases to 89.22 MW. When the gust wind covers the other rows of wind turbine generators with a delay time of 13.66 s, the generated active power at PCC bus is fluctuated between 82.37 and 89.4 MW before it returns to steady state

Table 5 Data of studied cases.

Cases	Pre-gust wind speed (m/s)	Distance (m)	Delay time (s)
Case 1	11	3D	13.66
		5D	22.77
		8D	36.44
Case 2	12	3D	12.67
		5D	21.12
		8D	33.76
Case 3	13	3D	11.81
		5D	19.69
		8D	31.48

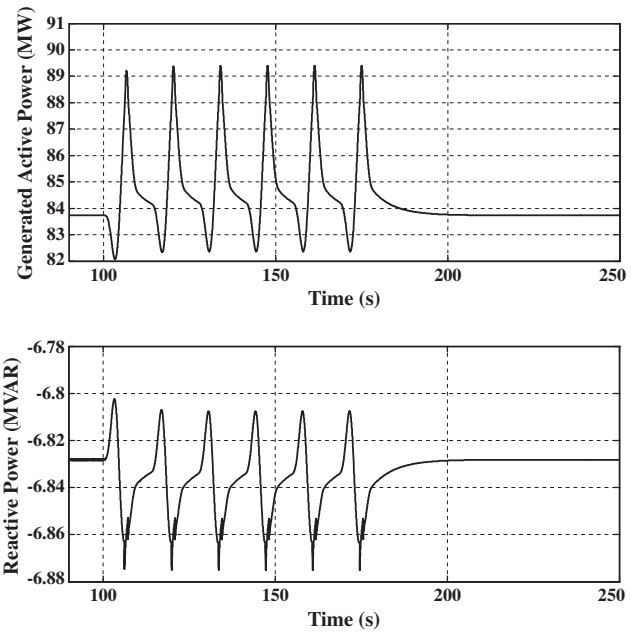

Figure 6 Active power and reactive power variations at PCC bus in case of gust wind based on hub wind speed of 11 m/s and distance equal to 3 times of rotor diameter.

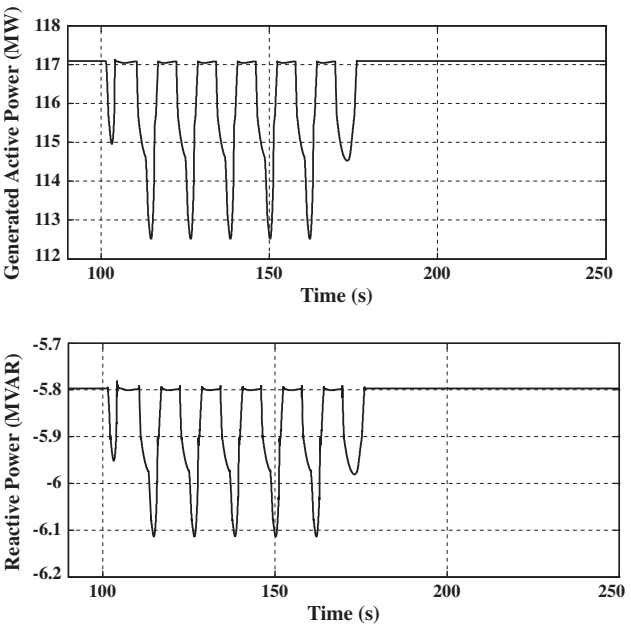

Figure 8 Active power and reactive power variations at PCC bus in case of gust wind based on hub wind speed of 13 m/s and distance equal to 3 times of rotor diameter.

value. Also, the absorbed reactive power at PCC bus is decreased to 6.802 MVAR, and then it increases to 6.875 MVAR when the gust wind covers wind turbine generators of row 1. When the gust wind covers the other rows with delay time of 13.66 s, the absorbed reactive power at PCC bus is fluctuated between 6.807 and 6.875 MVAR and then it returns to steady state value.

In case of gust wind speed variation based on 12 m/s, the wind speed is fluctuated between 9.79 and 18.09 m/s. In this case, the gust wind covers the rows of wind turbine generators with a delay time of 12.67 s. The generated active power at PPC bus is decreased to 106.6 MW, and then it increases to 110.2 MW when the gust wind covers wind turbine generators of row 1. When the gust wind covers the other rows with delay

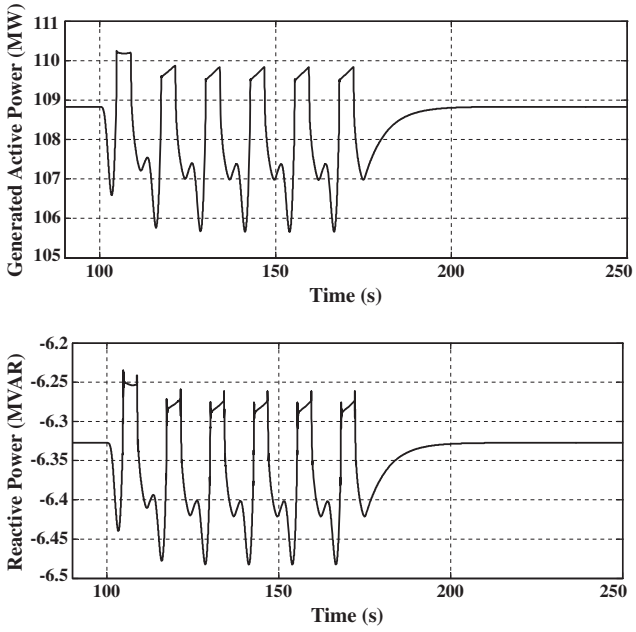

Figure 7 Active power and reactive power variations at PCC bus in case of gust wind based on hub wind speed of 12 m/s and distance equal to 3 times of rotor diameter.

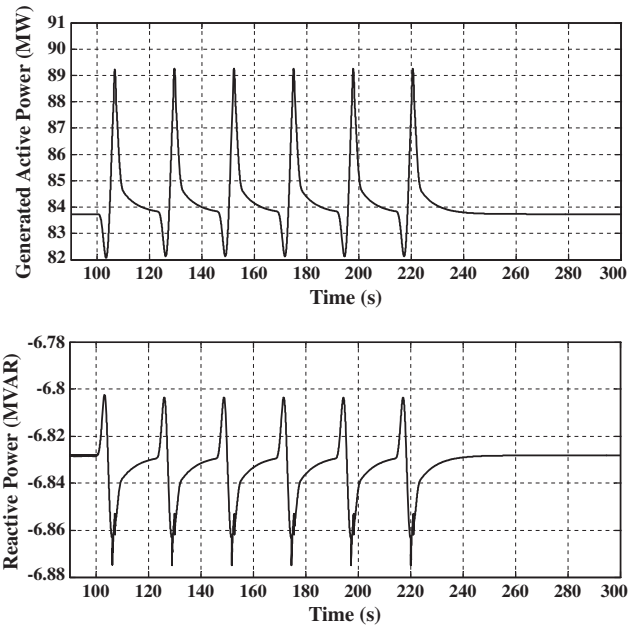

Figure 9 Active power and reactive power variations at PCC bus in case of gust wind based on hub wind speed of 11 m/s and distance equal to 5 times of rotor diameter.

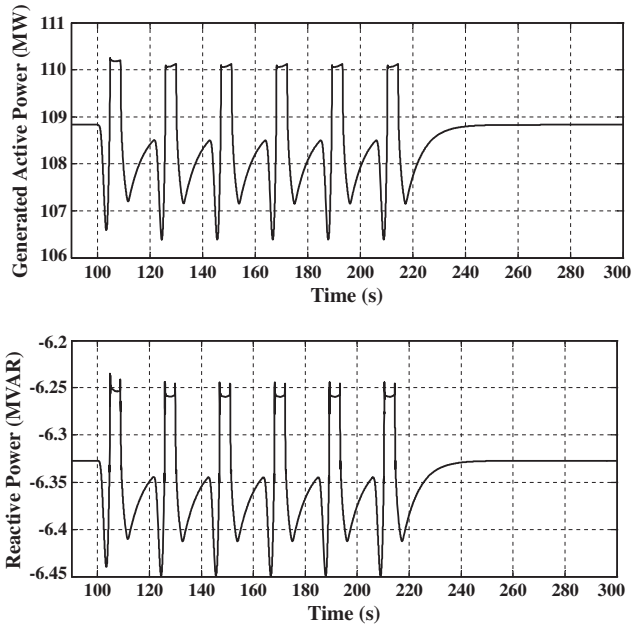

Figure 10 Active power and reactive power variations at PCC bus in case of gust wind based on hub wind speed of 12 m/s and distance equal to 5 times of rotor diameter.

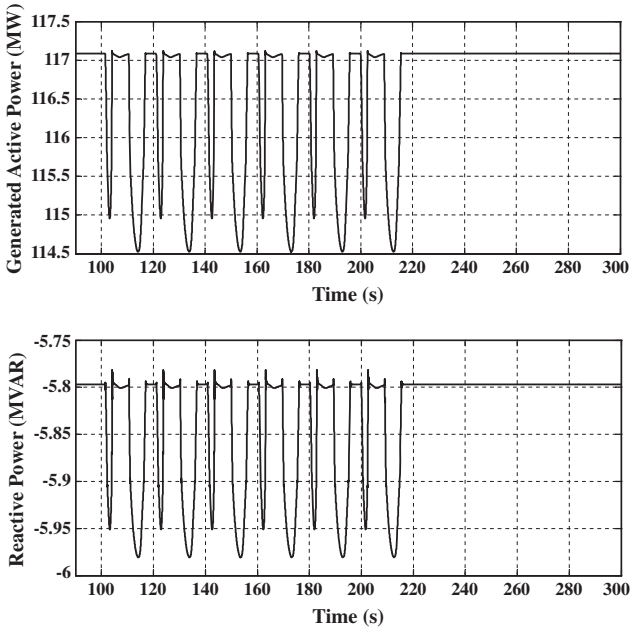

Figure 11 Active power and reactive power variations at PCC bus in case of gust wind based on hub wind speed of 13 m/s and distance equal to 5 times of rotor diameter.

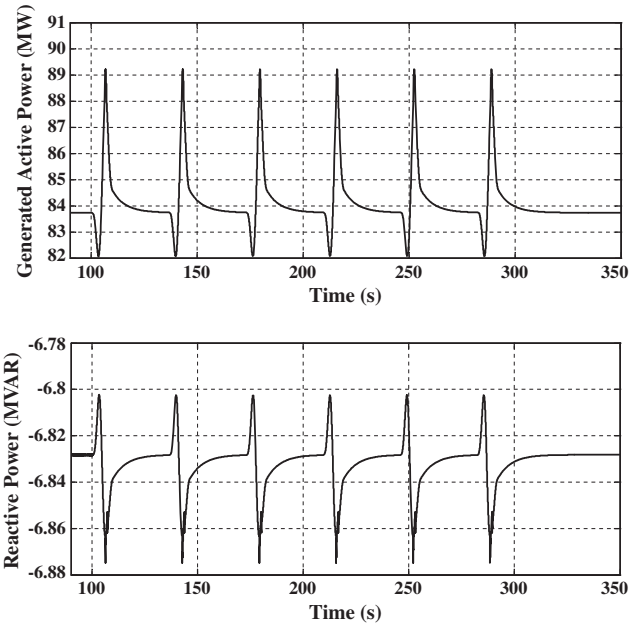

Figure 12 Active power and reactive power variations at PCC bus in case of gust wind based on hub wind speed of 11 m/s and distance equal to 8 times of rotor diameter.

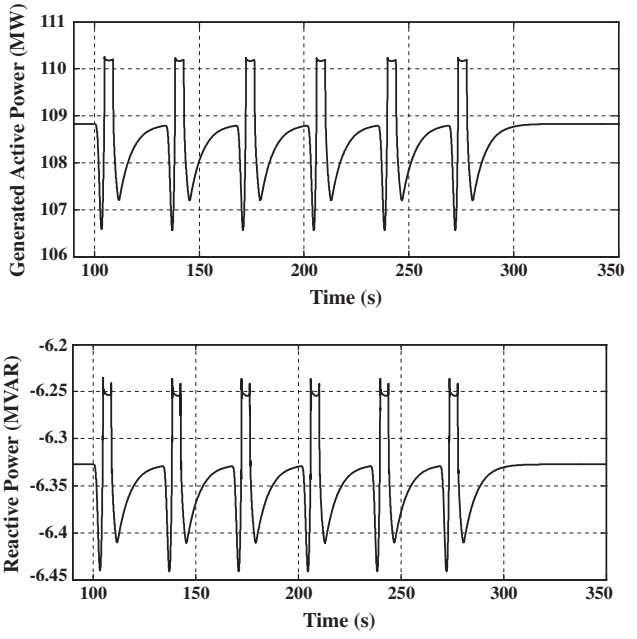

Figure 13 Active power and reactive power variations at PCC bus in case of gust wind based on hub wind speed of 12 m/s and distance equal to 8 times of rotor diameter.

time of 12.67 s, the active power is fluctuated between 105.7 and 109.9 MW, and then it returns to steady state value after gust wind passing. Also, the absorbed reactive power is increased to 6.44 MVAR, and then it decreases to 6.235 MVAR when the gust wind covers wind turbine generators of row 1, where it is fluctuated between 6.48 and 6.26 MVAR when the gust wind covers the other rows.

When the wind farm operates at rated wind speed of 13 m/s and the gust wind occurs based on it, the wind speed is fluctuated between 10.68 and 19.41 m/s and the delay time of gust wind to cover the rows of wind turbine generators is decreased to 11.81 s. When gust wind covers wind turbine generators of row 1, the generated active power at PCC bus is decreased to 115 MW by decreasing of gust wind speed. When the gust

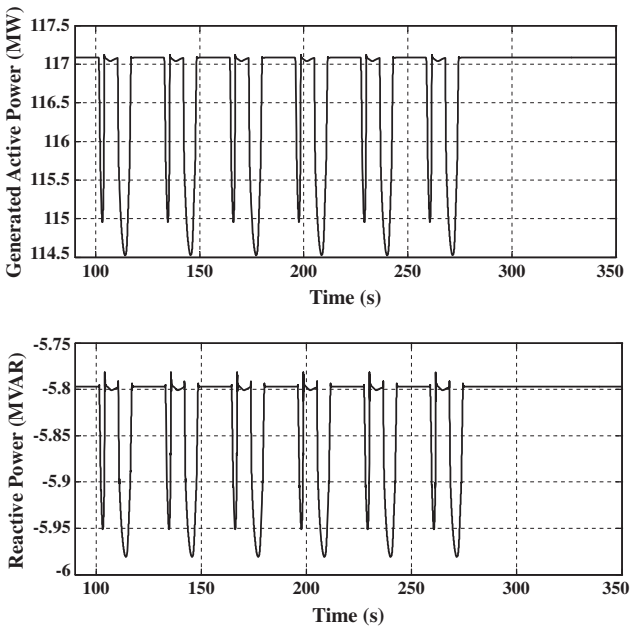

Figure 14 Active power and reactive power variations at PCC bus in case of gust wind based on hub wind speed of 13 m/s and distance equal to 8 times of rotor diameter.

wind speed is increased, the pitch angle control system limits the generated active power at it is rated value of 117.1 MW. When the gust wind covers the other rows of wind turbine generators, the generated active power is fluctuated between 112.5 MW and the rated value of 117.1 MW, then it returns to steady state after gust wind passing. Also the absorbed reactive power is not increased than that rated value of 5.797 MVAR during increasing the gust wind speed. When the gust wind speed covers wind turbine generators of row 1, the absorbed reactive power is increased to 5.95 MVAR by decreasing gust wind speed. Also, it is fluctuated between 6.11 MVAR and its steady state value when the gust wind covers the other rows.

By increasing the distance between wind turbine generator rows to 5 and 8 times of rotor diameter, the delay time of gust wind to cover the different wind turbine generator rows is increased. Also, the fluctuation behavior of generated active power and absorbed reactive power at PCC bus is affected. Figs. 9–11 show the variations in generated active power and absorbed reactive power at PCC bus when the distance between wind turbine rows equals to 5 times of rotor diameter. It is clear that, the variation in the generated active power and absorbed reactive power fluctuations at PCC bus is nearly the same for all wind turbine rows during gust wind passing. In case of gust wind based on pre-gust wind speed of 11 m/s, the generated active power is fluctuated between 82.13 and 89.2 MW, while the absorbed reactive power is fluctuated between 6.802 and 6.875 MVAR. Also, In case of gust wind based on pre-gust wind speed of 12 m/s, the generated active power is fluctuated between 106.6 and 110.2 MW, while the absorbed reactive power is fluctuated between 6.44 and 6.235 MVAR. When the wind farm operates at rated wind speed of 13 m/s, then gust wind occurs, the difference between fluctuation values of generated active power and absorbed reactive power is decreased during gust wind passing. The generated active power is fluctuated between 114.5 and 117.1 MW and the absorbed reactive power is fluctuated between 5.797 and 5.98 MVAR. As shown in Figs. 12–14, when the distance between wind turbine generator rows is increased from 5 to 8 times of rotor diameter, the fluctuation of generated active power and absorbed reactive power at PCC bus is not affected, but the system can return to steady state conditions after gust wind passing one wind turbine generator row and before it arrives the next. Fig. 15 shows the percentage active and reactive power fluctuation values for different studied cases where they are calculated based on maximum and minimum values of them during gust passing. When the distance between rows equals to 3 times of rotor diameter, the percentage active power fluctuation values equal to 8.7%, 4.1% and 3.9% for the gust occur based on wind speed of 11, 12 and 13 m/s respectively. By increasing the distance between rows to 5

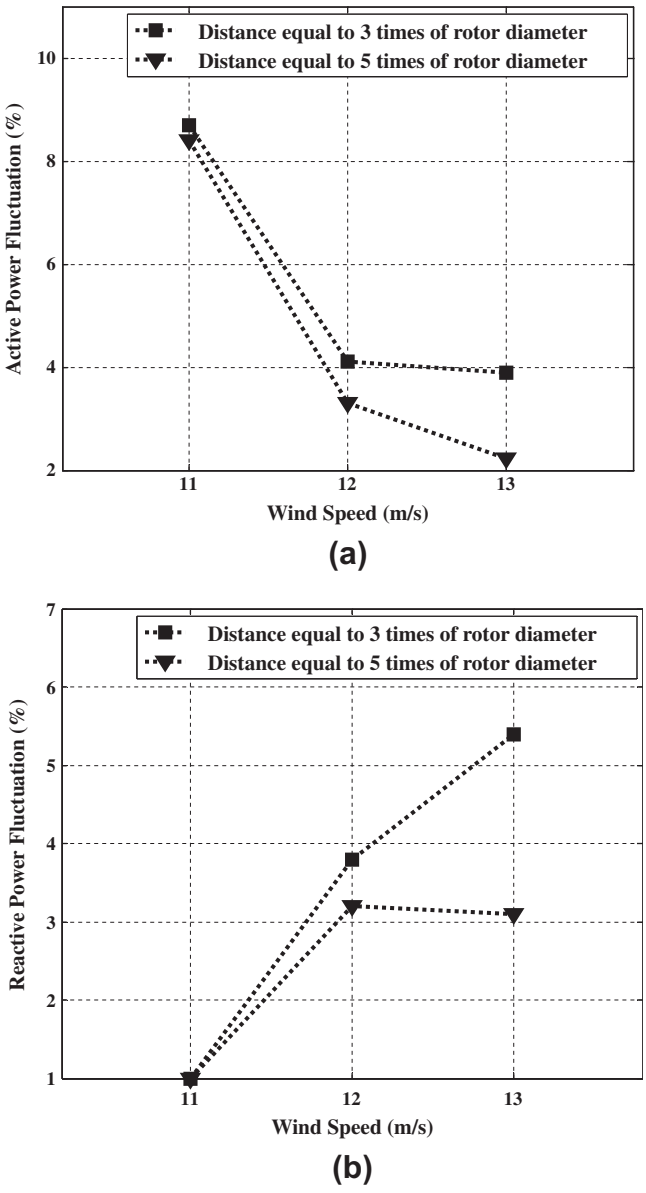

Figure 15 Percentage power fluctuations during gust wind passing. (a) Active power. (b) Reactive power.

times of rotor diameter, the percentage active power fluctuation values are decreased to 8.4%, 3.3% and 2.22% when the gust occurs based on wind speed of 11, 12 and 13 m/s respectively. It is clear that, the percentage active power fluctuation values are decreased by increasing the pre-gust wind speed and the distance between rows. As shown in Fig. 15(b), the percentage fluctuation of reactive power is increased by increasing the pre-gust wind speed and it decreases by increasing the distance between rows.

6. Conclusion

A simulation model of the under implementation 120 MW wind farm, located at Gulf El-Zayt, Red sea, Egypt, is investigated for studying the fluctuations of active and reactive power during extreme gust wind occurrence. The simulated wind farm is equipped with Doubly Fed Induction Generators and it consists of 60 wind turbines positioned in regular array of 10 by 6 where, 10 wind turbines are located in a row. A commercial 2 MW wind turbine generator with rotor diameter of 76.42 m, hub height of 70 m and rated wind speed of 13 m/s is used in this study. The extreme gust wind is simulated based on average wind speed over one-year period at Gulf El-Zayt site and the standard of IEC 61400-1. The extreme gust wind speed variations are simulated based on different pre-gust wind speeds of 11, 12, 13 m/s for studying the power fluctuations at different gusts. Also, the power fluctuations are studied during extreme gust wind occurrence for different distances between wind turbine rows equal to 3, 5 and 8 times of rotor diameter. These fluctuations are investigated by monitoring the active and reactive power at Point of Common Coupling bus PCC of the wind farm during different operation conditions. The percentage values of power fluctuation are calculated based on maximum and minimum values of them during gust passing. The results conclude that, the percentage active power fluctuation is decreased by increasing pre-gust wind speed, also it decreases by increasing the distance between wind turbine rows. It is noticed that, when the wind farm operates at pre-gust wind speed of 13 m/s and distance between rows equal to 5 times of rotor diameter, the percentage active power fluctuation is decreased by 46% comparing with the case of distance between rows equal to 3 times of rotor diameter. On the other hand, the percentage reactive power fluctuation is increased by increasing pre-gust wind speed, while it decreases by increasing the distance between wind turbine rows. When the wind farm operates at pre-gust wind speed of 13 m/s and distance between rows equal to 5 times of rotor diameter, the percentage reactive power fluctuation is decreased by 42.6% comparing with the case of distance between rows equal to 3 times of rotor diameter. The percentage fluctuation of active power and reactive power is not affected by increasing the distance between wind turbine rows from 5 to 8 times of rotor diameter. From the simulation and investigation, it can be observed that the wind turbine of class 1 with distance between turbines rows not less than 5 times of rotor diameter is appropriate for Gulf El-Zayt site.

References

[1] Quaschning V. Understanding renewable energy systems. London: Earthscan; 2005.

[2] Grady SA, Hussainia MY, Abdullah MM. Placement of wind turbines using genetic algorithms. Renew Energy 2005(30):259–70.

[3] Wharton S, Lundquist J, Sharp J, Zulauf M. Dependence of wind turbine curves on atmospheric stability regimes – an analysis of a west coast North American tall wind farm. American Geophysical Union Meeting, USA; 2009.

[4] New and Renewable Energy Authority (NREA) Annual Report; 2011.

[5] Wind turbine generator systems, Part 1, Safety requirements. IEC 61400-1; 1998. p. 328–37.

[6] Bierbooms W, Cheng PW, Larsen G, Pedersen BJ. Modelling of extreme gusts for design calculations-New Gust. Report JOR3-Ct98-0239, IW-00170R. Delft University of Technology; 2001.

[7] Ahmed Shata AS, Hanitsch R. The potential of electricity generation on the east coast of Red Sea in Egypt. Renew Energy 2006;31:1597–615.

[8] Rizk M. Wind characteristics and the available wind energy in Egypt. Solar Wind Technol 1987;4(4):491–9.

[9] Ministry of electricity and energy – New and Renewable Energy Authority (NREA) – Annual Report 2010/2011. <http://www.nrea.gov.eg>.

[10] Wikov-Wind W2000. 2MW wind turbine. Data sheet from Wikov Wind, www.wikov.com.

[11] Alaboudy AHK, Daoud AA, Desouky SS. Converter controls and flicker study of PMSG-based grid connected wind turbines. Sci Direct, Ain Shams Eng J 2013(4):75–91.

[12] El-Samanoudy M, Ghorab AAE, Youssef ShZ. Effect of some design parameters on the performance of a Giromill vertical axis wind turbine. Sci Direct Ain Shams Eng J 2010(1):85–95.

[13] Livani H, Bandarabadi M, Alinejad Y. Improvement of fault ride-through capability in wind farms using VSC-HVDC. Eur J Sci Res 2009;28(3):328–37.

[14] Noureldeen O, Rihan M, Hasanin B. Stability improvement of fixed speed induction generator wind farm using STATCOM during different fault locations and durations. Sci Direct Ain Shams Eng J 2011(2):1–10.

[15] El-Sattar AA, Saad NH, Shams El-Dein MZ. Dynamic response of doubly fed induction generator variable speed wind turbine. Sci Direct Electr Power Syst Res 2008(78):1240–6.

[16] Noureldeen O. Characteristics of fixed speed wind turbines interconnected grid during wind speed variations. In: 13th Middle East power systems conference MEPCON; 2009. p. 220–5.

[17] Rashad A, Noureldeen O, Wahab MAA. Behaviour of mixed wind farm based on SCIG and DFIG during wind gust occurence. In: 15th Middle East power systems conference MEPCON; 2012. p. 1–8.

[18] Slootweg JG. Wind power – modeling and impact on power system dynamic. PhD dissertation. Delft University, Netherlands; 2003.

[19] Giroux P, Sybille G, Le-Huy H. Modeling and simulation of a distribution STATCOM using simulink's power system blockset. In: 27th Annual conference of the IEEE industrial electronics society (2), USA; 2001. p. 990–4.

[20] Abdelfatah M, El-Shimy M, Ismail HM. Reliability analysis of 220 kV power transformers in Egypt. Sci Direct Ain Shams Eng J 2011:183–94.

[21] Perdana A. Dynamic models of wind turbines. PhD thesis. Chalmers University of Technology, Goeteborg, Sweden; 2008.

[22] Ganti VC, Singh BS, Aggarwal SK, Kandpal TC. DFIG-based wind power conversion with grid power leveling for reduced gusts. IEEE Trans Sustain Energy 2012;3(1):12–20.

[23] Hughes FM, Anaya-Lara O, Jenkins N, Strbac G. Control of DFIG-based wind generation for power network support. IEEE Trans Power Syst 2005;20(4):1958–66.

[24] Wang L, Wang KH. Dynamic stability analysis of a DFIG-based offshore wind farm connected to a power grid through an HVDC link. IEEE Trans Power Syst 2011;26(3):1501–10.

[25] Gonzalez-Longaat F, Wall P, Terzija V. Wake effect in wind farm performance: steady-state and dynamic behavior. Renew Energy 2012;39(1):329–38.

Omar Noureldeen is an assistant professor in the department of electrical engineering, Faculty of Engineering, Qena, South Valley University, Egypt. He received his Ph.D. in electrical power and machines from Faculty of Engineering, Cairo University in 2004. From 2004 to 2006, He has been assistant professor at the department of electrical engineering, Higher Institute of Energy, South Valley University. Since 2007, He is assistant professor at the department of electrical engineering, Faculty of Engineering – Qena, South Valley University. His fields of interest are digital protection of power systems, power system stability, and renewable energy systems.

Ahmed Rashad is an engineer in Upper Egypt Electricity Distribution Company, Qena Rural Electrification Sector, Egypt. His fields of interest are power system stability and renewable energy systems.